ISSN 0974 - 9373

Vol. 23 No. 2 (2019) **Journal of International Academy of Physical Sciences** pp. 143- 155

Evolution of Scale Factor with Cosmic Time while a Homogeneous Universe is Considered

Promila Biswas

Department of Mathematics
University of Burdwan, Purba Burdwan−713104, India.
Email:promilabiswas8@gmail.com

(Received October 17, 2018)

Abstract: We treat our universe as a homogeneous and isotropic system which is filled up by exotic matter popularly named as dark energy. Different dark energy models have been considered. The equation of continuity and the time - scale factor relations for different EoS-s of different dark energy models have been studied. Time vs scale factor relations are plotted for different dark energy models. We know that different dark energy models show different properties while occurrences of future singularities are considered. Those properties can be supported by the graphical analysis of their cosmic time-scale factor studies.

Keywords: Dark Energy, Scale Factor, Redshift parametrization.

1. Introduction

Einstein's famous field equation $G_{\mu\nu} = \frac{8\pi G}{c^4} T_{\mu\nu}$ relates the space-time curvature with the stress energy which originates from the presence of the matter in the concerned space-time. In earlier studies, models of our universe were taken as a homogeneous and isotropic system on a large scale. Firstly, the solution of this equation predicted that our universe is expanding but to support Einstein's belief that our universe is not static, he forcefully added a constant term Λ to the left hand side of the equation, i.e., with the geometric part of this equation to keep Einstein's model of universe static. Then $G_{\mu\nu} + \Lambda g_{\mu\nu} = \frac{8\pi G}{c^4} T_{\mu\nu}$ can be treated as a modification of gravity. When the constant term is taken with stress energy part, i.e., at the

right hand side of the equation, $G_{\mu\nu} = \frac{8\pi G}{c^4} T_{\mu\nu} - \Lambda g_{\mu\nu}$ can be treated as an introduction of exotic matter in cosmological studies.

After a short interval of time from Einstein's proposition of general relativity and proposal of Friedmann equations, Hubble's discovery showed that distant galaxies are moving away from us. This observation shows that our universe is expanding. Einstein aborted the constant term Λ from his equation. But to justify recent day observation of late time cosmicacceleration[1], constant term $\Lambda = -1$ is treated as the best supported cosmological model till date for such accelerated expansion[2].

When Friedmann-Lemaitre-Robertson-Walker (FLRW) metric for our universe described as homogeneous and isotropic, the derivation of Einstein's equation for the metric allows the violation of strong energy condition i.e., $\rho + 3p < 0$ and weak energy condition $\rho + p < 0$, i.e., to justify the late time cosmic acceleration where ρ is the energy density and p is the pressure respectively. Satisfying all these scenarios we will choose such equation of state (EoS) of an exotic fluid which is homogeneously distributed all over the universe and endeavors negative pressure as $p = \omega\rho$. This equation indicates the radiation era ($\omega = 1/3$), pressureless dust era ($\omega = 0$), quintessence era ($-1 < \omega < -1/3$) and phantom era ($\omega < -1$) accordingly as we change the value of the EoS parameter ω. As we can treat p, ρ and ω as a function of redshift z different redshift parameterizations of EoS parameters can be proposed.

Two recognized families of redshift parameterizations are following :

(i) Family I: $\omega(z) = \omega_0 + \omega_1 \left(\frac{z}{1+z}\right)^n$ and

(ii) Family II: $\omega(z) = \omega_0 + \omega_1 \frac{z}{(1+z)^n}$,

where ω_0 and ω_1 are two unresolved parameters, $n \in N$, the set of natural numbers. We will discuss particular redshift parameterizations (some of them satisfying the above mentioned families) in the next section. The best homogeneous and isotropic cosmological model is depicted by FLRW metric the form of which is given below, $(c = 1)$

$$dS^2 = \frac{a^2(t)}{\left(1+\frac{k_0 r^2}{4}\right)^2}\left[dr^2 + r^2 d\theta^2 + r^2 \sin^2\theta d\phi^2\right] - dt^2 . \tag{1.1}$$

Here $k_0 = 0, 1, -1$ indicate that the universe is flat, closed and open respectively. Now the field equations and the continuity equation are respectively[3] :

$$\begin{cases} \frac{2\ddot{a}}{a} + \frac{\dot{a}^2 + k_0}{a^2} = -kp + \Lambda, \\ 3\left(\frac{\dot{a}^2 + k_0}{a^2}\right) = k\rho + \Lambda, \\ \dot{\rho} + 3\frac{\dot{a}}{a}(\rho + p) = 0. \end{cases} \tag{1.2}$$

Combining we obtain,

$$\frac{\dot{a}^2}{2} - \left(\frac{4\pi\rho}{3} + \frac{\Lambda}{6}\right)a^2 = -\frac{k_0}{2} . \tag{1.3}$$

Equation (1.3) is the conservation equation of the total energy of the universe, where $\dot{a}^2/2$ is the kinetic energy and $\left(\frac{4\pi\rho}{3} + \frac{\Lambda}{6}\right)a^2$ is the gravitational potential energy. From equations (1.1), (1.2) and (1.3) we obtain the general solution of the system. We define a function

$$M(\rho) = \exp\left[\int \frac{d\rho}{\rho + p}\right] > 0 , \tag{1.4}$$

or

$$\frac{dM(\rho)}{d\rho} = \frac{M(\rho)}{\rho + p} > 0 ,$$

$$\Rightarrow M(\rho)a^3 = m_0$$

,[m_0 is constant] by the help of the equation of continuity. We will apply the above theoretical basement and the mathematical constructions for different dark energy models in the next section.

2. Mathematical Construction of Different Redshift Parameterization Models of Dark Energy to Analyse Corresponding Physical Properties

Model I: For $n=0$ of family II, we get the EoS of Linear parameterization[4], i.e.,

$$p(z)=(\omega_0+\omega_1 z)\rho(z). \tag{2.1}$$

Now from (1.3) and (1.4), we get the result for Linear Parameterization as follows,

$$\dot{a}^2=2\left\{\frac{4\pi}{3}\left(m_0a^{-3}\right)^{(1+\omega_0+\omega_1 z)}+\frac{\Lambda}{6}\right\}a^2-k_0. \tag{2.2}$$

Solving t for $a(t)$ we get,

$$t-t_0=\int\left[2\left\{\frac{4\pi}{3}\left(m_0a^{-3}\right)^{(1+\omega_0+\omega_1 z)}+\frac{\Lambda}{6}\right\}a^2-k_0\right]^{-\frac{1}{2}}da. \tag{2.3}$$

To find an analytic solution of the equation (2.3), here we assume $\omega_0=-1$, $\omega_1=0$, $m_0=1$ and we have the solutions :

$$k_0=0,\quad t(a)=\sqrt{\left(\frac{3}{8\pi-1}\right)}\ln a, \tag{2.4}$$

$$k_0=1,\quad t(a)=\sqrt{\left(\frac{3}{8\pi-1}\right)}\ln\frac{a\sqrt{8\pi-1}-\sqrt{a^2(8\pi-1)-3}}{a\sqrt{8\pi-1}+\sqrt{8\pi-4}}, \tag{2.5}$$

$$k_0=-1,\quad t(a)=\sqrt{\left(\frac{3}{8\pi-1}\right)}\left(\sinh^{-1}\left[\sqrt{\frac{8\pi-1}{3}}\right]+\sinh^{-1}\left[a\sqrt{\frac{8\pi-1}{3}}\right]\right) \tag{2.6}$$

Now we are going to plot t vs $a(t)$ graph for $k_0 = 0, 1$ and -1 for the equation (2.3) numerically in figures 1a, 1b and 1c respectively.

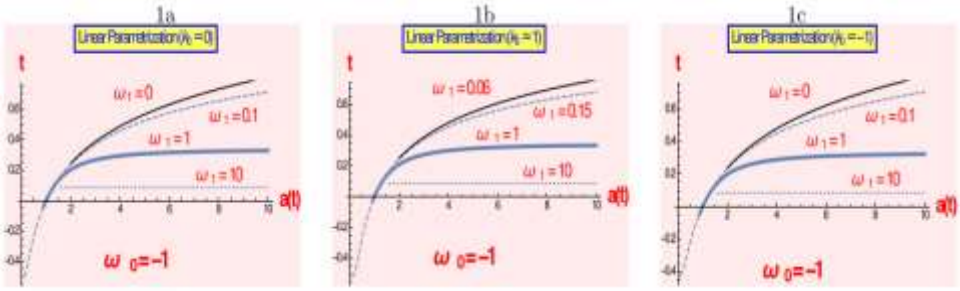

Figure 1a-1c. Plots of t w. r. t. $a(t)$ for linear parametrization for $k_0 = 0$ and 1, -1 respectively

We see the scale factor is steeply increasing as time increases. Keeping $\omega_0 = -1$ fix, if we increase the value of ω_1, scale factor blows up quickly for lower values of t. As time increases, z and $\omega_0 + \omega_1(z)$ both go to the negative zone. This increases the negativity in the pressure via the increment in scale factor's value.

Model II : For $n = 1$ in family I and II, we get the EoS of Chevallier and Polarski (CPL) parameterization, i.e.

$$p(z) = \left\{\omega_0 + \frac{\omega_1 z}{1+z}\right\}\rho(z). \tag{2.7}$$

This ansatz was first introduced by Chevallier and Polarski[5] and later discussed by Linder[6]. For SNeIa data set the best fit values for CPL are $\omega_0 = 1.58$ and $\omega_1 = 3.29$.

For CPL, we get similar result from equations (1.3) and (1.4) as follows,

$$\dot{a}^2 = 2\left\{\frac{4\pi}{3}\left(m_0 a^{-3}\right)^{\left(1+\omega_0+\frac{\omega_1 z}{1+z}\right)} + \frac{\Lambda}{6}\right\}a^2 - k_0,$$

$$t - t_0 = \int \left[2\left\{ \frac{4\pi}{3}\left(m_0 a^{-3}\right)^{\left(1+\omega_0+\frac{\omega_1 z}{1+z}\right)} + \frac{\Lambda}{6} \right\} a^2 - k_0 \right]^{-\frac{1}{2}} da \,. \tag{2.8}$$

again we will plot t vs $a(t)$ for the equation (2.8) keeping $\omega_0 = -1$ always in figures 2a, 2b and 2c for $k_0 = 0, 1$ and -1 respectively.

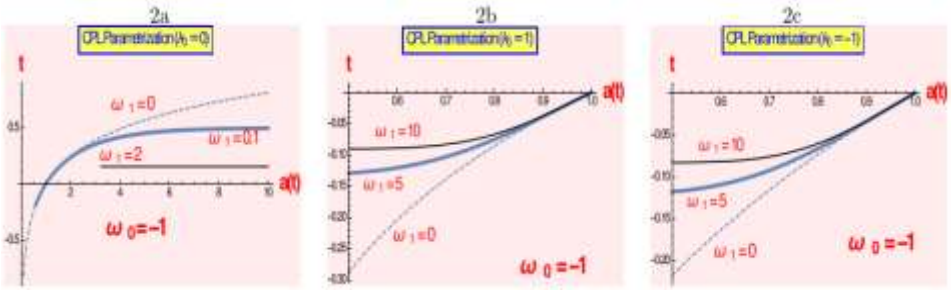

Figure 2a-2c. Plots of t w. r. t. $a(t)$ for CPL parametrization for $k_0 = 0$ and 1, -1 respectively

We have plotted the $t - a(t)$ graphs for different ω_1 in the case of flat universe, i.e., $k_0 = 0$, the time graph is high for small values of $a(t)$ or we can say as $a(t)$ increases, the rate of increment of t decreases. The rate is decreasing of t is high for higher values of ω_1. In the case of closed universe, we have plotted three ω_1 cases, i.e., $\omega_1 = 0, 5$ and 10. Here we can see the time increases rapidly accordingly to the value of $a(t)$. For lower values of $a(t)$, the time graph is noticeably different. But for the higher value of $a(t)$, the $t - a(t)$ graphs are almost the same. In the region $-0.145 < \omega_1 < -0.12$, time increment goes strictly high $a(t) > 0.9$. In the case of the open universe, similar phenomena happen, but the time region changes. For figure 2(c) we have chosen all the values same as above. We can see only the time region is different here.

Model III : For $n = 2$, it gives the EoS of Jassal-Bangla-Padmanabhan (JBP) Parameterization[7], i.e.,

$$p(z) = \left\{ \omega_0 + \frac{\omega_1 z}{(1+z)^2} \right\} \rho(z) \,. \tag{2.9}$$

Same as above two models we will solve for t using equation (1.3) and (1.4) we get,

$$\dot{a}^2 = 2\left\{\frac{4\pi}{3}\left(m_0 a^{-3}\right)^{\left(1+\omega_0+\frac{\omega_1 z}{(1+z)^2}\right)} + \frac{\Lambda}{6}\right\}a^2 - k_0 ,$$

$$t - t_0 = \int\left[2\left\{\frac{4\pi}{3}\left(m_0 a^{-3}\right)^{\left(1+\omega_0+\frac{\omega_1 z}{(1+z)^2}\right)} + \frac{\Lambda}{6}\right\}a^2 - k_0\right]^{-\frac{1}{2}} da . \tag{2.10}$$

Similarly as previous, we will plot $t - a(t)$ graphs using equation (2.10) in figures 3a, 3b and 3c for $k_0 = 0, 1$ and -1 respectively.

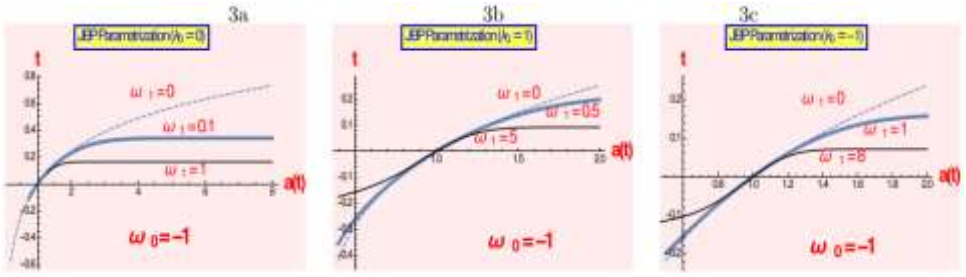

Figure 3a-3c. Plots of t w. r. t. $a(t)$ for JPB parametrization for $k_0 = 0$ and 1, -1 respectively

For all the graphs fixing, ω_0 as -1 and have plotted the graphs for $k_0 = 0, 1$ and -1. In fig 3a, we can see for higher values of ω_1, time graph is decreasing and tends to almost parallel to $a(t)$ axis. In fig 3b and 3c, i.e., in the case of a closed and open universe we can notice that same phenomena happen. The time graph increases then it becomes constant in a region and finally decreases for the ascending values of ω_1. For both the cases the time region of the remaining constant is the same.

Model IV : The EoS takes the form as[8],

$$p(z) = \left\{\omega_0 + \omega_1 \ln(1+z)\right\}\rho(z) . \tag{2.11}$$

We will call it Efstathiou parameterization.

Proceeding as similar manner solving for t from equation (1.3) and (1.4) we get,

$$\dot{a}^2 = 2\left\{\frac{4\pi}{3}\left(m_0 a^{-3}\right)^{\left(1+\omega_0+\omega_1\ln(z+1)\right)} + \frac{\Lambda}{6}\right\}a^2 - k_0,$$

(2.12) $$t - t_0 = \int\left[2\left\{\frac{4\pi}{3}\left(m_0 a^{-3}\right)^{\left(1+\omega_0+\omega_1\ln(z+1)\right)} + \frac{\Lambda}{6}\right\}a^2 - k_0\right]^{-\frac{1}{2}} da\,.$$

Now we will plot the similar graphs in figures 4a, 4b and 4c for $k_0 = 0, 1$ and -1 respectively.

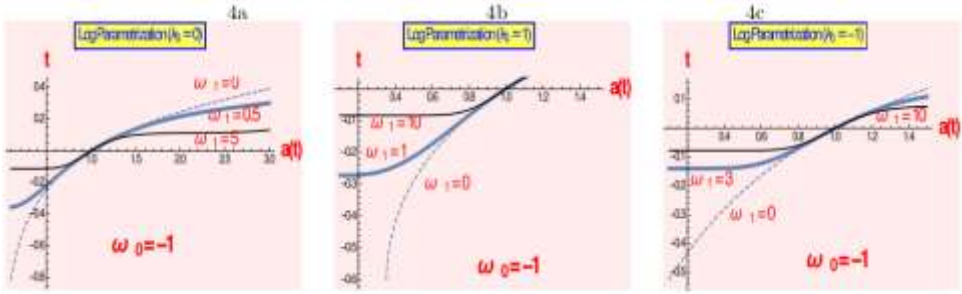

Figure 4a-4c. Plots of t w. r. t. $a(t)$ for Logarithmic parametrization for $k_0 = 0$ and 1, -1 respectively

In fig 4a, keeping $\omega_0 = -1$, we can see that atfirst t starts from negative, then it remains the same for all values of ω_1 and after that its negativity decreases and it enters on a positive scale. Here we can notice the region range for t is $-0.08 < t < 0.05$ for $0.9 < a(t) < 1.2$ In fig 4b, keeping $\omega_0 = -1$, the increment of time was quite different and it increases according to the higher values of ω_1. As we increase the value of t and ω_1, the $a(t)$ graph is also increasing. In fig 4c, the same phenomenon like fig 4a happens. In the range of $0.9 < t < 1.15$, the time increment is same for all values of ω_1.

Model V : The EoS is given as[9,10],

(2.13) $$p(z) = \left\{-1 + \frac{(1+z)}{3}\frac{A_1 + 2A_2(1+z)}{A_0 + 2A_1(1+z) + A_2(1+z)^2}\right\}\rho(z).$$

This redshift parameterization is exactly the cosmological constant for $A_1 = A_2 = 0$ and DE models when $\omega = -\frac{2}{3}$ for $A_0 = A = 0$ and $\omega = \frac{1}{3}$ for $A_0 = A_1 = 0$. For SNeIa gold data set the best fit values of A_1 and A_2 are 4.16 and 1.67 respectively. We will call this parameterization as Alam-Sahni-Saini-Starobinski (ASSS) parameterization.

Then using equations (1.3) and (1.4) and equation from (2.13) we will solve for t and get,

$$\dot{a}^2 = 2\left\{\frac{4\pi}{3}\left(m_0 a^{-3}\right)^{\frac{3}{(1+z)}\frac{A_0+2A_1(1+z)+A_2(1+z)^2}{A_1+2A_2(1+z)}} + \frac{\Lambda}{6}\right\}a^2 - k_0,$$

$$t - t_0 = \int\left[2\left\{\frac{4\pi}{3}\left(m_0 a^{-3}\right)^{\frac{3}{(1+z)}\frac{A_0+2A_1(1+z)+A_2(1+z)^2}{A_1+2A_2(1+z)}} + \frac{\Lambda}{6}\right\}a^2 - k_0\right]^{-\frac{1}{2}} da \qquad (2.14)$$

Again we will plot $t - a(t)$ graph using equation (2.14) in figures 4a, 4b and 4c for $k_0 = 0, 1$ and -1 respectively.

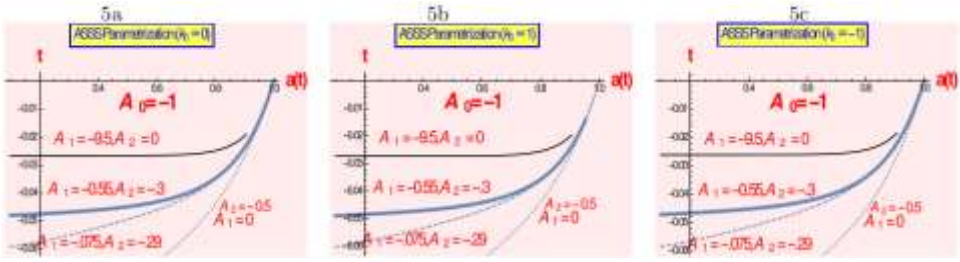

Figure 5a-5c. Plots of t w. r. t. $a(t)$ for ASSS parametrization for $k_0 = 0$ and 1, -1 respectively

In this parameterization all the cases are nearly the same. The increment of time graph is strictly high and constant, when $a(t) > 0.95$. For lower values of $|A_1|$ and $|A_2|$, (i.e., which may show similar phenomenon to the ΛCDM case) , the slope of $t - a(t)$ is high. But for higher values of $|A_1|$, $|A_2|$ and lower values of $a(t)$, we get time graph almost parallel to $a(t)$ axis. Increasing the values of $|A_1|$ and $|A_2|$, the graph are more parallel to

$a(t)$ axis for low $a(t)$. For confinely we can conclude for low t, i.e., the early universe has grown older, $a(t)$ converging to a finite value. This model disobeys the Big Rip theory. For $k_0 = 1$, $k_0 = -1$ we can find similar nature as $k_0 = 0$ case

Model VI : We introduce another redshift parameterization which also contains an adjustable initial parameter ω. We will discuss her about Generalised Cosmic Chaplygin Gas (GCCG)[11] model whose EoS takes the form as

$$p = \rho^{-\alpha}\left[C + \left(\rho^{1+\alpha} - C\right)^{-\omega}\right]. \tag{2.15}$$

Similar way, using equations (1.3) and (1.4) we get from equation (2.15) we get,

$$\dot{a}^2 = 2\left\{\frac{4\pi}{3}\left[\left\{\left(m_0 a^{-3}\right)^{(\omega+1)(\alpha+1)} - 1\right\}^{\frac{1}{1+\omega}} + C\right]^{\frac{1}{\alpha+1}} + \frac{\Lambda}{6}\right\}a^2 - k_0,$$

$$t - t_0 = \int\left[2\left\{\frac{4\pi}{3}\left[\left\{\left(m_0 a^{-3}\right)^{(\omega+1)(\alpha+1)} - 1\right\}^{\frac{1}{1+\omega}} + C\right]^{\frac{1}{\alpha+1}} + \frac{\Lambda}{6}\right\}a^2 - k_0\right]^{-\frac{1}{2}} da\,. \tag{2.16}$$

Again proceeding the similar manner as above we will solve the equation (2.16) numerically for finding $t - \alpha(t)$ graphs.

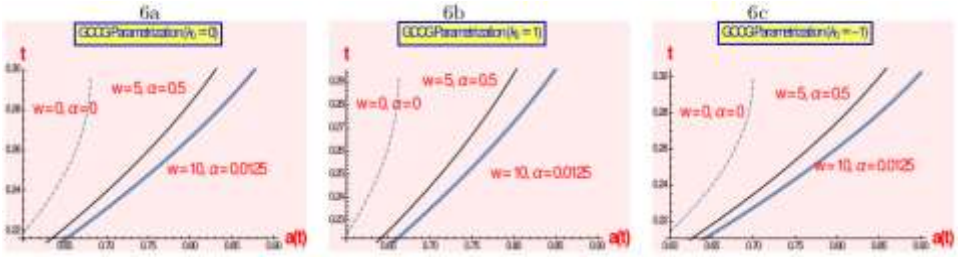

Figure 6a-6c. Plots of t w. r. t. $a(t)$ for GCCG parametrization for $k_0 = 0$ and 1, -1 respectively

In the case of GCCG, we can notice that three cases are almost same except their time range for ω and α. When $\alpha=\omega=0$, i.e., for ΛCDM case, we see the time graph is increasing. For low $a(t)$, t goes slowly and then it increases rapidly and diverges to finite $a(t)$. This means, scale factor does not blow to infinity and always stays finite. The slope of $t-a(t)$ curve decreases for higher values of ω and α. But we will find finite $a(t)$ for finite domain t. The same trend is carried for an enclosed and open universe. This redshift parameterization does not allow a future singularity and the graphs also support the pre established result.

3. Brief Discussions and Conclusions

In this article we have studied the evolution of time t and scalar factor $a(t)$ when our present day universe is experiencing a late time cosmic acceleration. To justify the effect of negative pressure employed by the exotic fluids filled in all over the universe is taken as homogeneous and isotropic, we have chosen different EoSs which are depending on redshift z and some arbitrary redshift parameters. In every case, we have fixed ω_0 as -1, then varied all other parameters accordingly the significant changes. At first, we have discussed the simplest method, i.e., linear redshift parameterization where we can see for three cases of k_0 if we choose smaller ω_0 and ω_1, the slope of $t-a(t)$ the curve is higher. This shows that linear parameterization supports strong cosmic acceleration and this may tend to a future singularity i.e., Big Rip. For CPL parameterization, the tendency of $t-a(t)$ the curve is the same as linear parameterization. If we increase t, the rate of $a(t)$ is not high as the linear parameterization case. The power of negative pressure is less comparable to linear parameterization. It speculates that the flat universe, i.e., for $k_0=0$, CPL behaves like highly negative pressure exerting gas. Otherwise we can say that CPL is more controllable than linear parameterization. For closed and open universe, i.e., for $k_0=-1,1$ the previous scenario changes completely. We see that $t-a(t)$ curves are almost constant for low $a(t)$ and it increases with increment of $a(t)$. For low t and low ω_1, high $a(t)$ is observed. For closed and open universe, the Big Rip does not occur in the future. In the case of JBP, the curves are finitely similar with linear parameterization. So

JBP is good to describe a future as well as a past singular singularity together. For Efstathiou parameterization, the same trends like JBP carry on. For ASSS parameterzation, we see the appropriate curves are available for past time only. For GCCG all these phenomena do not occur. For low α and ω, as we increase $a(t)$, we can notice t blowing up. Even this says about an infinite time to find a finite scale factor. Increasing ω, we observe the curves to increase but it never goes parallel to the $a(t)$ axis. For high t, $a(t)$ must converge to some finite values. This means no future singularity is allowed in the GCCG model.

Acknowledgements: The Author thanks the Department of Higher Education, Science & Technology and Biotechnology, West Bengal for providing Swami Vivekananda Merit-Cum-Means Scholarship..

References

1. S. Perlmutter, G. Aldering, S. Deustua, S. Fabbro, G. Goldhaber, D. E. Groom, A. G. Kim, M. Y. Kim, R. A. Knop, P. Nugent, C. R. Pennypacker, A. Goobar, R. Pain, I. M. Hook, C. Lidman, R. S. Ellis, M. Irwin, R. G. McMahon, P. Ruiz-Lapuente, N. Walton, B. Schaefer, B. J. Boyle, A.V. Filippenko, T. Matheson, A. S. Fruchter, N. Panagia, H. J. M. Newberg and W. J. Couch, (The Supernova Cosmology Project), Cosmology from Type Ia Supernovae, *Bull. Am. Astron. Soc*., **29** (1997), 1351.

2. T. Padmanabhan, The Atoms of Spacetime and the Cosmological Constant, *Journal of Physics: Conf. Series*, **880** (2017), 012008.

3. A. K. Raychaudhuri, S. Banerjee and A. Banerjee, *General Relativity, Astrophysics, and Cosmology*, Springer - Verlag, New York, 1992.

4. A. R. Cooray and D. Huterer, Gravitational Lensing as a Probe of Quintessence, *Astrophys. J. Lett.*, **513** (1999), L95-L98.

5. A. Upadhye, M. Ishak and P. Steinhardt, Dynamical Dark Energy: Current Constraints and Forecasts, *Phys. Rev. D*, **72** (2005), 063501.

6. M. Chevallier and D. Polarski, Accelerating Universes with Scaling Dark Matter, *Int. J. Mod. Phys. D*, **10** (2001), 213-223.

7. H. K. Jassal, J. S. Bagla and T. Padmanabhan, WMAP Constraints on Low Redshift Evolution of Dark Energy, *Mon. Not. Roy. Astron. Soc.*, **356** (2005), L11-L16.

8. G. Efstathiou, Constraining the Equation of State of the Universe from Distant Type Ia Supernovae and Cosmic Microwave Background Anisotropies, *Mon. Not. Roy. Astron. Soc.*, **310** (1999), 842-850.

9. U. Alam, V. Sahni, T. D. Saini and A. A. Starobinski, Is there Supernova Evidence for Dark Energy Metamorphosis?, *Mon. Not. Roy. Astron. Soc.*, **354** (2004a), 275-291.

10. U. Alam, V. Sahni and A. A. Starobinski, The Case for Dynamical Dark Energy Revisited, *JCAP*, **0406** (2004), 008 .

11. Pedro F. González-Díaz, You Need Not Be Afraid of Phantom Energy, *Phys. Rev. D*, **68** (2003), 021303.